E3Sym: Leveraging E(3) Invariance for Unsupervised 3D Planar Reflective Symmetry Detection
Supplementary Material

Ren-Wu Li[1,2] Ling-Xiao Zhang[1] Chunpeng Li[1*] Yu-Kun Lai[3] Lin Gao[1,2]

[1]Beijing Key Laboratory of Mobile Computing and Pervasive Device,
Institute of Computing Technology, Chinese Academy of Sciences
[2]University of Chinese Academy of Sciences
[3] School of Computer Science and Informatics, Cardiff University

renwuli1024@gmail.com, {zhanglingxiao, cpli, gaolin}@ict.ac.cn, LaiY4@cardiff.ac.uk

1. Validation on Real-World Data

To validate the ability of our method to detect symmetries in real-world scenarios, we test our method on reconstructed or raw scanned models. The visualization results are displayed in Figure 1, the left is a sofa reconstructed by NeuS [7], and the right is a raw scanned chair in ScanNet [3]. Despite the presence of artifacts on the sofa and the chair is incomplete (the right leg connection is missing), and the shapes are not completely symmetric, our method can detect acceptable symmetries, demonstrating its effectiveness and robustness.

(a) (b)

Figure 1: Results on reconstructed or raw scanned models. (a) a sofa reconstructed by NeuS [7], (b) a raw scanned chair in ScanNet [3].

2. Rotational Symmetry Reasoning

As Chertok et al. proposed in their 2D image symmetry detection work [2], two distinct reflection transforms can determine a unique corresponding rotational transform. For a 3D shape with multiple reflective symmetries detected, the shape might be rotational symmetric. To eliminate detecting excessive planar reflective symmetries for rotational symmetric shapes, we can recover the corresponding rotational symmetry from detected symmetry planes. To be specific, for each pair of distinct reflective transforms from detected planar reflective symmetries i and j: $\mathbf{T}^i_{\text{ref}}$ and $\mathbf{T}^j_{\text{ref}}$, the corresponding rotational transform can be recovered as $\mathbf{T}^{ij}_{\text{rot}} = \mathbf{T}^i_{\text{ref}} \cdot \mathbf{T}^j_{\text{ref}}$. Figure 2 provides examples for rotational symmetry reasoning, the left one is an octahedron with 13 rotation axes and the right are four shapes sharing continuous rotational symmetry, the recovered rotational axes are highlighted in red for visualization. Note that all rotational axes of octahedron are reasoned because our method is able to detect an arbitrary number of reflective symmetry planes, showing the effectiveness of the proposed approach.

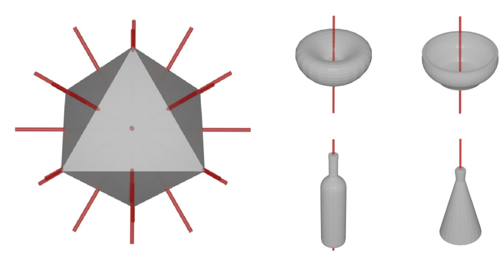

Figure 2: Our method can detect reasonable rotational symmetries.

*Corresponding author

Method	PCA	OBB	Kazhdan et.al.	Martinet et.al.	Mitra et.al.	PRST	PRST with GEDT	Korman et.al.	PRS-Net	Ours
GTE($\times 10^{-2}$)	2.41	1.24	0.17	13.6	52.1	4.42	3.97	19.2	0.11	**0.09**

Table 1: The GTE ($\times 10^{-2}$) measured with different methods on ShapeNet [1].

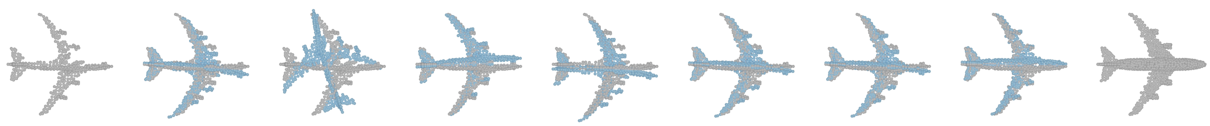

(a) Input	(b) PCA	(c) OBB	(d) Kormal et al.	(e) PRST	(f) PRST with GEDT	(g) PRS-Net	(h) Ours	(i) GT
	4.5	11.7	2.2	6.2	3.6	7.8	1.8	

Figure 3: Comparison of shape completion. The symmetry parts are mirrored by the detected symmetry planes and are highlighted in light blue. The Chamfer distances ($\times 10^{-4}$) between the completed point cloud and ground truth point cloud are displayed underneath the completion results, our method achieves the lowest Chamfer distance. Please zoom in to see more details.

3. Application to Shape Completion

As useful high-level information, symmetry can be useful in a wide variety of applications. We apply symmetry detection to shape completion in this case. After obtaining the symmetries of an incomplete shape, we can reasonably restore its missing parts. Figure 3 shows a comparison of our method against baselines, the input incomplete point cloud is a randomly rotated airplane (for better visualization, we rotate it back in Figure 3), the symmetry parts are mirrored according to the detected symmetry planes and are highlighted in light blue. The Chamfer distances ($\times 10^{-4}$) between the completed point cloud and ground truth point cloud of different methods are displayed on the bottom as well, our method achieve the lowest Chamfer distance.

4. Additional Results

4.1. Quantitative results

Following PRS-Net [5], GTE (Ground Truth Error) is also adopted as a metric, which measures how close the predicted symmetry is to the corresponding ground truth. Due to the directional ambiguity of a plane, the error is computed as:

$$\mathrm{GTE}(S, S_{gt}) = \min(\mathrm{MSE}(S, S_{gt}), \mathrm{MSE}(-S, S_{gt})), \quad (1)$$

where S_{gt} is the ground truth symmetry of S and MSE is the mean squared error. Quantitative results compared with baseline methods are listed in Table 1, which shows that our method outperforms other methods in GTE as well.

4.2. Qualitative results

Additional qualitative reflective symmetry detection results in ShapeNet compared with different methods are shown in Fig. 4. Our method is able to detect all valid planar reflective symmetries, while other methods detect redundant or inaccurate planes, showing the effectiveness of our method. In Figs. 5, 6, 7, additional visualization results in 12 categories of ShapeNet are displayed to further demonstrate the effectiveness to detect symmetries for different shapes.

4.3. Comparison with Vector Neurons

We evaluate our method compared with the novel Vector Neurons (VN) [4] that can produce rotation invariant features from point clouds on MVP [6]. We replace the encoder in our framework with VN-PointNet for feature extraction. The method of Vector Neurons [4] gets 10.17 for SDE and 12.54 for SDE*, where SDE* measures the performance when the incomplete shape is randomly rotated. Apart from that the extracted features of our method perform better than Vector Neurons [4] (see Table 3 in the main paper), benefiting from the end-to-end unsupervised framework we proposed, the performance of our framework with the encoder replaced by VN-PointNet still outperforms the previous state-of-the-arts by a large margin, e.g., PRS-Net [5] that achieves 34.10 for SDE and 46.13 for SDE* respectively.

References

[1] Angel X Chang, Thomas Funkhouser, Leonidas Guibas, Pat Hanrahan, Qixing Huang, Zimo Li, Silvio Savarese, Manolis Savva, Shuran Song, Hao Su, et al. ShapeNet: An information-rich 3D model repository. *arXiv preprint arXiv:1512.03012*, 2015. 2

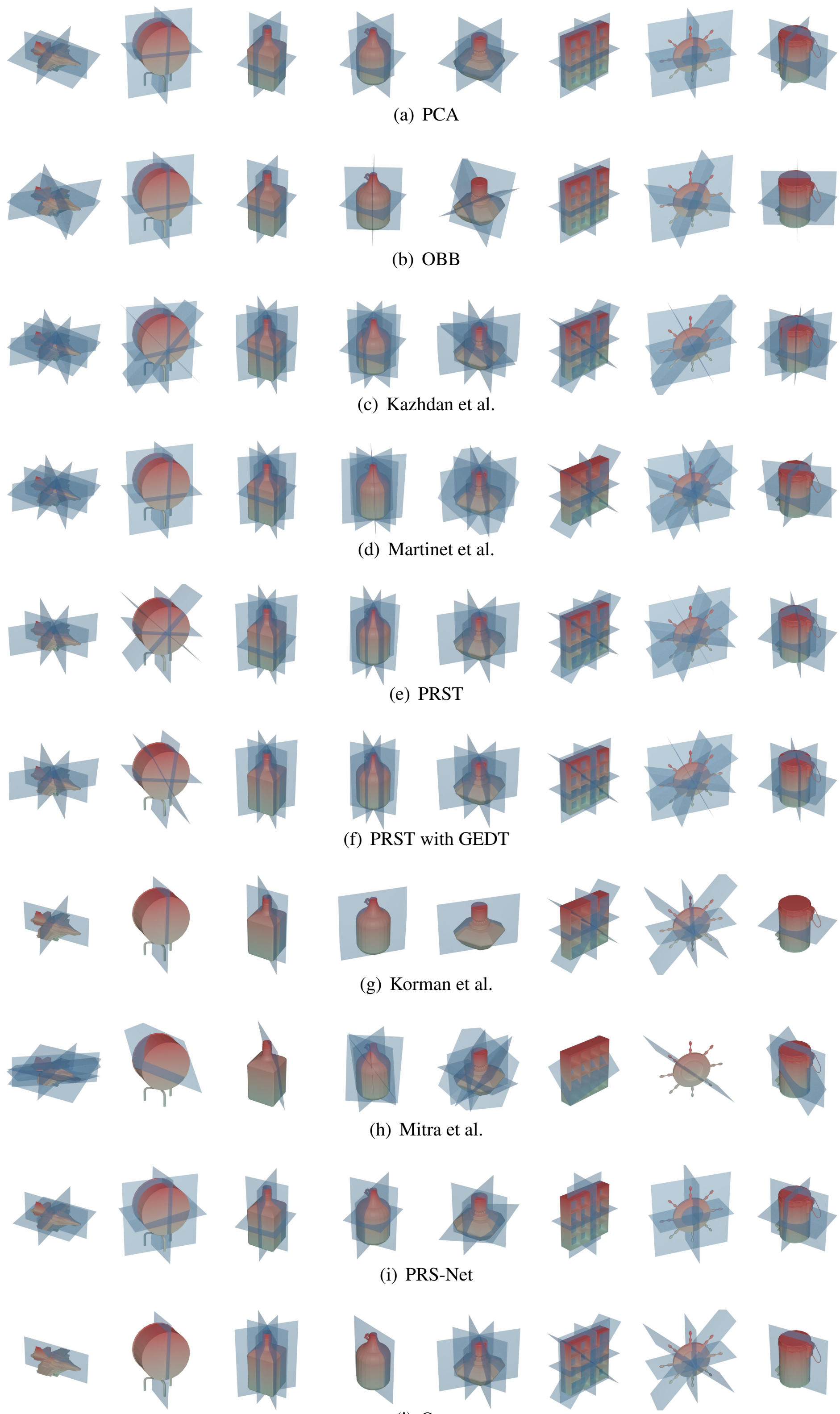

(a) PCA

(b) OBB

(c) Kazhdan et al.

(d) Martinet et al.

(e) PRST

(f) PRST with GEDT

(g) Korman et al.

(h) Mitra et al.

(i) PRS-Net

(j) Ours

Figure 4: Qualitative reflective symmetry detection results in ShapeNet comparing different methods.

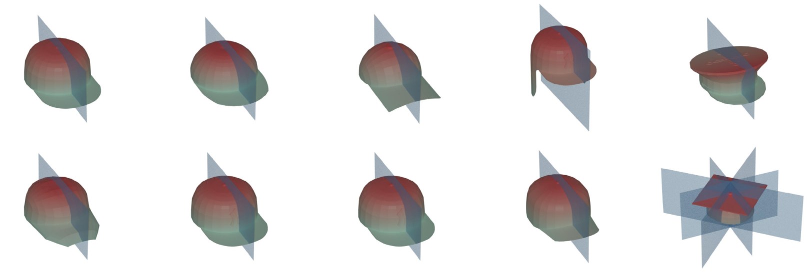

(a) Cap

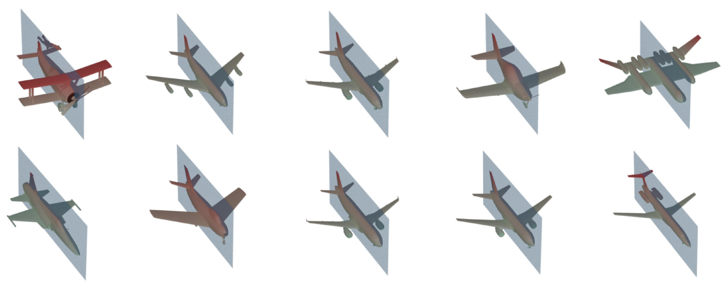

(b) Airplane

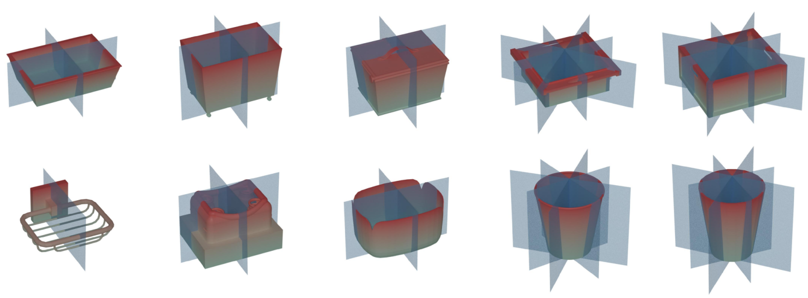

(c) Basket

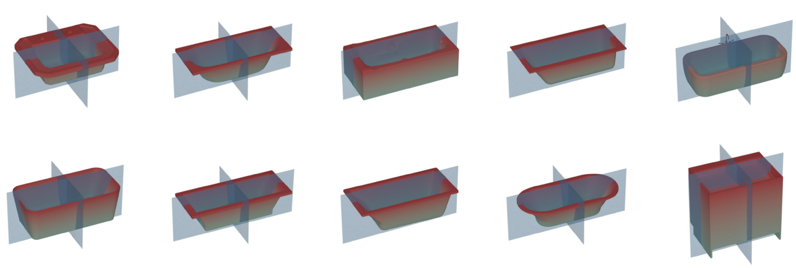

(d) Bathtub

Figure 5: Qualitative reflective symmetry detection results in ShapeNet, including (a) Cap, (b) Airplane, (c) Basket, (d) Bathhub.

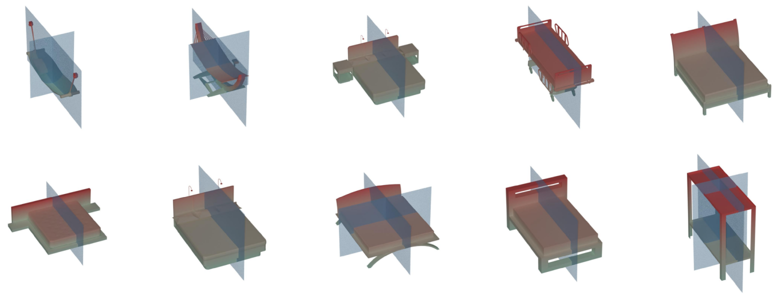

(a) Bed

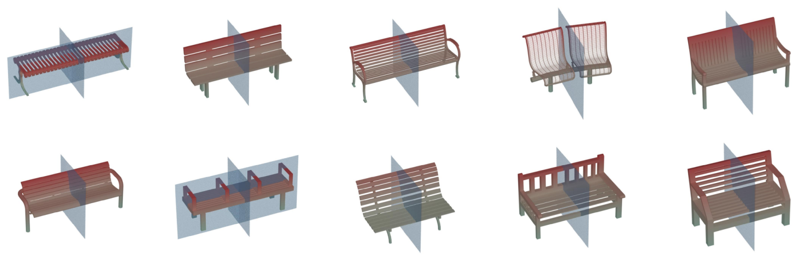

(b) Bench

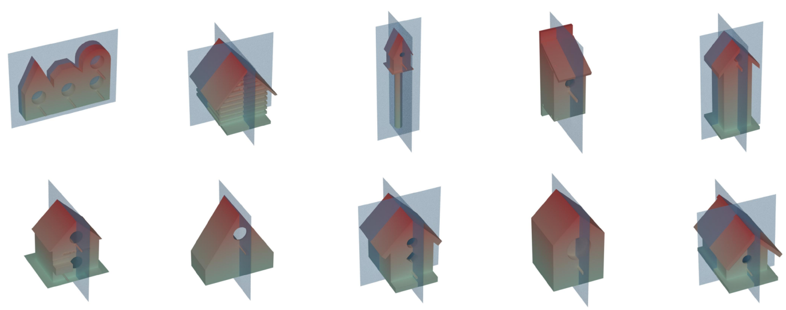

(c) Bird House

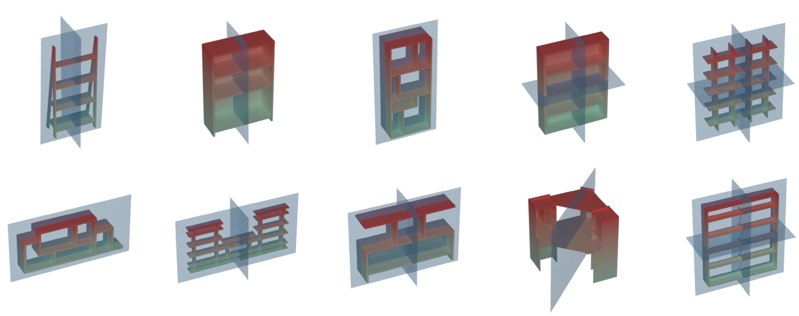

(d) Book Shelf

Figure 6: Qualitative reflective symmetry detection results in ShapeNet, including (a) Bed, (b) Bench, (c) Bird House, (d) Book Shelf.

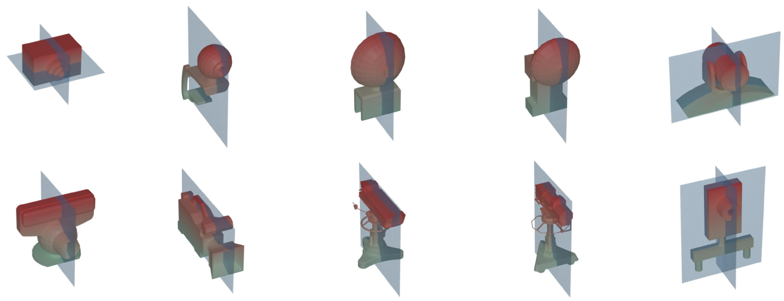

(a) Camera

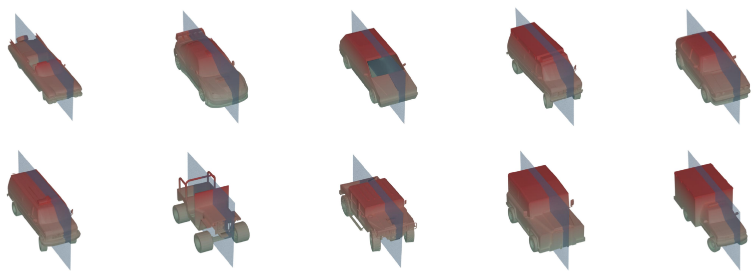

(b) Car

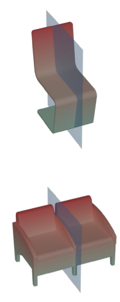

(c) Chair

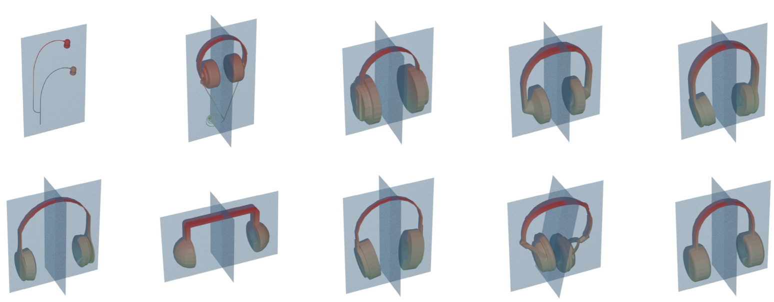

(d) Earphone

Figure 7: Qualitative reflective symmetry detection results in ShapeNet, including (a) Camera, (b) Car, (c) Chair, (d) Earphone.

[2] Michael Chertok and Yosi Keller. Spectral symmetry analysis. *IEEE Transactions on Pattern Analysis and Machine Intelligence*, 32(7):1227–1238, 2010. 1

[3] Angela Dai, Angel X Chang, Manolis Savva, Maciej Halber, Thomas Funkhouser, and Matthias Nießner. ScanNet: Richly-annotated 3D reconstructions of indoor scenes. In *Proceedings of the IEEE conference on computer vision and pattern recognition*, pages 5828–5839, 2017. 1

[4] Congyue Deng, Or Litany, Yueqi Duan, Adrien Poulenard, Andrea Tagliasacchi, and Leonidas Guibas. Vector neurons: A general framework for so(3)-equivariant networks. In *2021 IEEE/CVF International Conference on Computer Vision (ICCV)*, pages 12180–12189, 2021. 2

[5] Lin Gao, Ling-Xiao Zhang, Hsien-Yu Meng, Yi-Hui Ren, Yu-Kun Lai, and Leif Kobbelt. PRS-Net: Planar reflective symmetry detection net for 3D models. *IEEE Transactions on Visualization and Computer Graphics*, 27(6):3007–3018, 2020. 2

[6] Liang Pan, Xinyi Chen, Zhongang Cai, Junzhe Zhang, Haiyu Zhao, Shuai Yi, and Ziwei Liu. Variational relational point completion network. In *Proceedings of the IEEE/CVF Conference on Computer Vision and Pattern Recognition*, pages 8524–8533, 2021. 2

[7] Peng Wang, Lingjie Liu, Yuan Liu, Christian Theobalt, Taku Komura, and Wenping Wang. NeuS: Learning neural implicit surfaces by volume rendering for multi-view reconstruction. *arXiv preprint arXiv:2106.10689*, 2021. 1